University of Groningen

Simulation of fracture of cementitious composites with explicit modeling of microstructural features

Tijssens, M.G.A.; Sluys, B.L.J.; van der Giessen, E.

IMPORTANT NOTE: You are advised to consult the publisher's version (publisher's PDF) if you wish to cite from it. Please check the document version below.

Document Version
Publisher's PDF, also known as Version of record

Publication date:
2001

Link to publication in University of Groningen/UMCG research database

Simulation of fracture of cementitious composites with explicit modeling of microstructural features

M.G.A. Tijssens [a,*], L.J. Sluys [a], E. van der Giessen [b]

[a] *Koiter Institute Delft, Delft University of Technology, Stevinweg 1, 2628 CN, Delft, The Netherlands*
[b] *Department of Applied Physics, University of Groningen, Nyenborgh 4, 9747 AG, Groningen, The Netherlands*

Abstract

Fracture of cementitious composites is analyzed numerically using the cohesive surface methodology. The presence of aggregates in the cement matrix is explicitly accounted for. The composite is modeled in two dimensions as a three-phase material, the third phase being the weak interfacial transition zone in between aggregates and cement matrix. The bulk material is regarded as elastic and fracture is described with cohesive surfaces. The cohesive surface constitutive model is motivated by experimental observations regarding the loading-rate sensitivity of cementitious composites and analytical studies regarding fracture of planar microcracks. The model predicts the important toughening mechanism of crack face bridging occurring in cementitious composites. © 2001 Published by Elsevier Science Ltd.

Keywords: Cohesive surfaces; Mesostructure; Concrete; Finite elements; Fracture mechanisms

1. Introduction

Concrete is a highly heterogeneous material. On the macroscale one typically observes large aggregates bonded by a matrix of mortar (see Fig. 1(a)). This mortar phase itself, hereafter to be called the mesolevel, consists of small aggregates and sand bonded by the cement paste (Fig. 1(b)). The cement paste consists of fully and partially hydrated cement grains and possibly larger voids (Fig. 1(c)). Upon further examination one may detect small cracks which originate for example from the shrinkage due to drying or due to autogenous shrinkage. Zooming further into the material, Fig. 1(d) reveals that the hydrated cement itself is a structure of cauliflower-like particles separated by voids and what remains of the needle-like structure of the calcium–silicate-hydrate (CSH) crystals. Besides the various constituents summarized above, the difference in properties of the various constituents in cement paste and interfacial transition zone (ITZ) further increases the heterogeneity of the mortar phase.

Fracture processes in concrete have been observed to be a continuous process of creating and linking up of microcracks. Due to the simultaneous growth of microcracks at different locations and the mutual

---

[*] Corresponding author. Tel.: +31-15-278-6602; fax: +31-15-278-6383.
E-mail address: m.g.a.tijssens@wbmt.tudelft.nl (M.G.A. Tijssens).

(a) (b)

(c) (d)

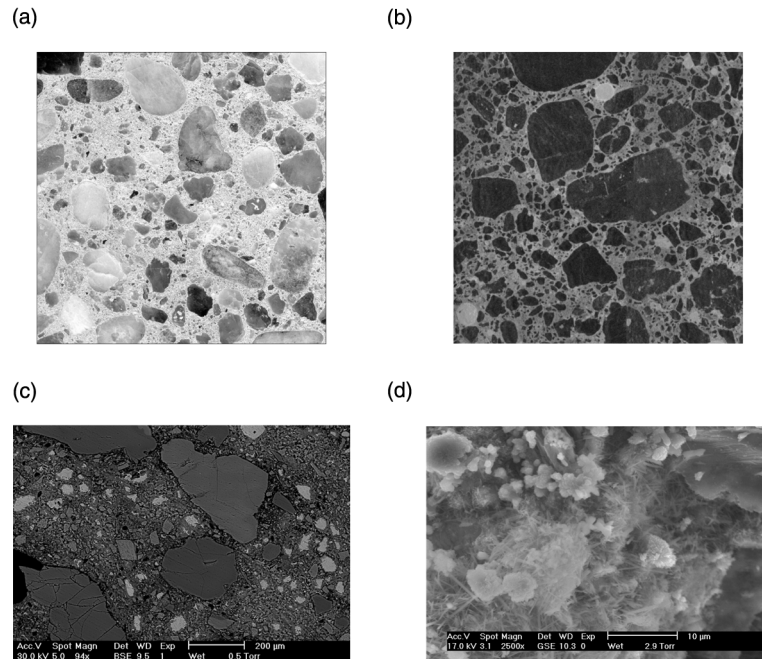
Fig. 1. Structure of concrete upon successively higher magnifications. (a) Normal concrete specimen, 7×7 cm^2, (b) 15×15 mm^2, (c) 1×0.8 mm^2 and (d) 0.05×0.04 mm^2.

avoidance of microcracks, bridges form between cracks. After an initial steep softening response these bridges result in a long tail in the load–displacement curve.

The modeling technique described in this paper attempts to describe fracture of a cementitious composite without a priori assuming the location of cracks. Despite the complexity of the microstructure of a cementitious composite, we assume that, on the mesolevel, it can be modeled as a three-phase material. The three phases are (i) the hardened cement paste, (ii) the aggregates and (iii) the weak ITZ separating the former two phases. The deformation of the bulk material is described by finite elements where we assume that aggregates do not fracture. Fracture of the cement paste and ITZ is accounted for by the use of cohesive surfaces. A cohesive surface relates the traction transmitted over the surface, to the separation between the surfaces.

The cohesive surface methodology, also known as the cohesive crack model, has been used in previous investigations regarding the fracture behavior of concrete [1–3]. These studies often are restricted to a single, fixed, crack path on the macroscale. Also, the traction-separation relation used for the cohesive crack is often fixed and has no relation with the physical mechanisms underlying the initiation and growth of the crack. The cohesive surface methodology can be exploited further though by modeling the physical mechanisms that give rise to the growth of cracks. Thus, the traction-separation relation of the cohesive surfaces themselves is not fixed a priori but may be a result of the fracture processes that have been taken into account. Using the multiple cohesive surface technique pioneered by Xu and Needleman [4], fracture of the cementitious composite will evolve solely depending on the material model used in the cohesive surfaces and the interaction with the intact, elastic, regions of the material.

Although it is often assumed that concrete can be modeled as a rate independent, elastic material, experimental evidence [5–10] shows that strain-rate effects cannot be neglected. Experiments indicate that moisture plays an important role but the origin of the strain-rate sensitivity of concrete is still subject to

debate. In this paper the constitutive response of a cohesive surface uses a local damage description in terms of a single damage parameter ω. Damage evolution in the cohesive surface model affects the ability to transmit tractions over the cohesive surface. The rate of change of the damage parameter is taken to be governed by the current state of stress and damage, giving rise to a strain-rate dependent response of the cohesive surface. Note that we implicitly assume that basic creep and fracture are both a result of growth of microcracks and both are captured in the damage evolution law for the cohesive surfaces. Complicating factors such as the Pickett effect, i.e. that the total creep during simultaneous drying and loading exceeds the sum of creep due to loading and shrinkage due to drying, are not accounted for. However, the separation of bulk constitutive response from fracture events using cohesive surfaces is particularly suited to study such more complicated, competing processes.

In Section 2 we will present the constitutive model for the cohesive surface. A combined analytical–numerical parametric study of a model system is given in Section 3. Results of this analysis are used in Section 4 in which results of detailed finite element calculations are given to analyze the effect of aggregate position, aggregate size distribution and loading rate on the global peak stress and fracture energy. Concluding remarks are given in Section 5.

2. Material model

Fracture of solids is a result of breaking of bonds on the molecular level. For this reason, inelastic deformation has often been described with the Tobolsky–Eyring relation [11]. Though originally proposed to describe the deformation and fracture characteristics of rubber-like materials, the Tobolsky–Eyring relation was verified by Zhurkov [12] for many other materials including metals and non-metallic crystals. It has been shown experimentally (see Ref. [10] for a review) that the rate dependence of the strength of concrete is similar to the rate dependence of the materials tested by Zhurkov [12]. A description of fracture of a cementitious composite in the same spirit as the Tobolsky–Eyring relation may therefore also be applicable.

Examining the microstructure of concrete, one observes that the heterogeneity on a mesolevel finds its origin in the presence of voids, sand and aggregates, partly and fully hydrated cement grains and microcracks (see Fig. 1). On a microscale one finds the needle-like structure of the CSH and calcium-hydrate crystals. Also the ITZ separating cement paste and non-hydraulic additives has a very complex structure (see, e.g., Ref. [13]). It can be expected that even for very small macroscopic loads, stress concentrations occur on the microlevel that cause microcracks to initiate and grow.

In this paper, all damage is concentrated in the cohesive surfaces. The bulk of the material is assumed to remain elastic. This is described by the well-known relation in terms of the second Piola–Kirchhoff stress $\boldsymbol{\tau} = \tau^{ij}\boldsymbol{e}_i\boldsymbol{e}_j$ and the Lagrangian strain $\boldsymbol{\eta} = \eta_{ij}\boldsymbol{e}^i\boldsymbol{e}^j$:

$$\dot{\tau}^{ij} = \mathscr{L}^{ijkl}\dot{\eta}_{kl} \tag{1}$$

in which $\mathscr{L}^{ijkl}$ is the modulus tensor for an isotropic elastic material expressed fully by Young's modulus E and Poisson's ratio v.

The growth of microcracks results in a deterioration of the elastic stiffness of the material. For this reason we propose to use a cohesive surface law of the form

$$\boldsymbol{T} = (1 - \omega)\boldsymbol{D}\boldsymbol{\Delta} \tag{2}$$

in which $\boldsymbol{T}$ and $\boldsymbol{\Delta}$ are the traction and separation vector of the cohesive surface and ω the damage variable. The elastic stiffnesses in normal and tangential direction, as described by $\boldsymbol{D}$, are assumed to be equal and uncoupled, i.e. $\boldsymbol{D} = k\boldsymbol{I}$, $\boldsymbol{I}$ being the unit matrix.

The three-dimensional interaction effects in a microcracked region of a material are rather complex and whether shielding or amplification occurs depends on the precise position and orientation of the

microcracks [14]. However, analytical studies regarding the interaction effects of planar microcracks on the intensity of the stress field [15,16] show that under constant load, the intensity increases as the distance between the microcracks becomes smaller. As we assume that the deterioration of the material can be described by lumping all fracture events in cohesive surfaces, we follow these analytical studies and disregard the possibility of shielding in a microcracked region.

Motivated by the heterogeneous nature of the microstructure of concrete and the analytical studies regarding planar microcracks, we propose to use a Tobolsky–Eyring-like relation to describe the rate of change of the damage variable ω according to

$$\dot{\omega} = \frac{\dot{\omega}_0}{(1-\omega)^n} \sinh\left(\frac{T_n}{T_0}\right)^m \tag{3}$$

in dependence of the traction component $T_n = \boldsymbol{T} \cdot \boldsymbol{n}$ normal to the cohesive surface. The influence of the material parameters $\dot{\omega}_0$, T_0, n and m are investigated next.

3. Behavior of a model system

To understand the behavior of the present cohesive surface model we study a one-dimensional model system consisting of a piece of elastic bulk material and a cohesive surface loaded in uniaxial tension by a uniform displacement field $\dot{u}$ (see Fig. 2).

In this case the cohesive surface traction T_n must necessarily be equal to the vertical stress component σ in the bulk material, i.e.,

$$\dot{\sigma} = E\dot{\epsilon} = \frac{E}{h}(\dot{u} - \dot{\Delta}_n) = \dot{T}_n. \tag{4}$$

From Eq. (2), the rate of the normal traction T_n is expressed as

$$\dot{T}_n = (1-\omega)k\dot{\Delta}_n - \dot{\omega}k\Delta_n \tag{5}$$

and by combining Eq. (3) with Eq. (5), one obtains the following non-linear differential equation governing the response of the model
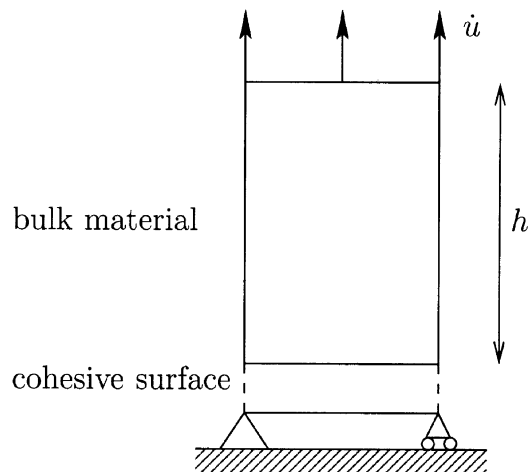

Fig. 2. Model system used to study the combined response of the elastic continuum and the cohesive surfaces.

$$\dot{T}_{n}\left(1 + (1 - \omega)\frac{kh}{E}\right) + \frac{\dot{\omega}_0 T_n}{(1 - \omega)^{n+1}}\sinh\left(\frac{T_n}{T_0}\right)^m = (1 - \omega)k\dot{u} \tag{6}$$

which must be solved simultaneously with Eq. (3). Introducing the dimensionless traction $y = T_n/T_0$ and the dimensionless time $\tau = \dot{\omega}_0 t$, the set of differential equations reads:

$$y'\left(1 + (1 - \omega)\frac{kh}{E}\right) + \frac{y}{(1 - \omega)^{n+1}}\sinh(y^m) = (1 - \omega)\frac{k}{T_0}u' \tag{7}$$

$$\omega' = \frac{1}{(1 - \omega)^n}\sinh(y^m) \tag{8}$$

in which $(\ )'$ denotes differentiation with respect to τ. The initial conditions are $y = 0$, $\omega = 0$ at $\tau = 0$.

Note that the response of the model system is governed by the driving force ku'/T_0 and the ratio kh/E. The latter involves a discussion on convergence in the cohesive surface methodology upon refining the discretization of the continuum. It also indicates that the constitutive model of cohesive surfaces is intimately linked to the length scale on which they are used. Here, we will use the cohesive surfaces on the mesolevel in concrete. The length scale h is therefore taken be equal to 1 mm, be it rather arbitrary. The precise value of the peak traction and fracture energy of the cohesive surface now depends on k/E. In order to limit the elastic deformation of the cohesive surfaces, we take $k/E = 2500$ mm^{-1}.

Using the explicit Euler forward integration rule, the set (7) and (8) is integrated numerically to obtain the response of the model system for various values of n and m. Especially the variation of the peak traction T_{peak} and the fracture energy G_f with n and m are of interest. It can easily be shown that the fracture energy can be obtained as

$$G_f = \int_0^{\Delta_n^{\max}} T_n\,d\Delta_n = T_0 u' \int_0^{\tau_{\max}} y\,d\tau \tag{9}$$

in which $\tau_{\max}$ is the dimensionless time at which full breakdown has occurred and in which we have assumed that all elastic energy has disappeared upon full breakdown.

From Eq. (7), one observes that when final failure approaches, the rate y' is governed by $\sinh(y^m)/y^n$. For $y \downarrow 0$ this can be approximated by y^{m-n}. We can thus conclude that there are three possible ways to attain breakdown, i.e. (i) accelerated breakdown for $m < n$, (ii) breakdown at constant rate $\dot{T}_n$ for $m = n$ and (iii) decelerated breakdown for $m > n$. The latter possibility is not relevant for quasi-brittle materials. The values of m and n are thus subject to the restriction $m \leqslant n$.

To obtain values for n and m that are representative for concrete, we study the relaxation behavior of the model system and compare this with experiments on three-point bend specimens of Bažant and Gettu [5]. To this end, we load the system until the traction reaches a value of 80% of the peak stress in the post-peak regime and keep the displacement u constant thereafter.

Figs. 3 and 4 show the development of the traction T_n/T_{peak} with time τ for various combinations of n and m. From Fig. 3 it is seen that if m is smaller then n, the stress continuous to drop down quickly once relaxation has started. The experiments done by Bažant and Gettu [5] on three-point bend specimens have shown that in the post-peak regime between 80% and 50% of the peak load, relaxation is nearly linear with the logarithm of time. Since various fracture processes in concrete may result in the observed relaxation behavior, one must be careful when comparing experiments with the model system. However, the predicted load relaxation of the model system should not deviate too much from linearity. We must therefore conclude that the model is only applicable to concrete if m and n are nearly equal.

The model system, of course, is very limited in representing realistic complex material systems in which the effects of e.g. moisture content and nearly strain-rate independent behavior of aggregates are important. Perhaps even more important is that within the cohesive surface model we assume that creep in concrete is a
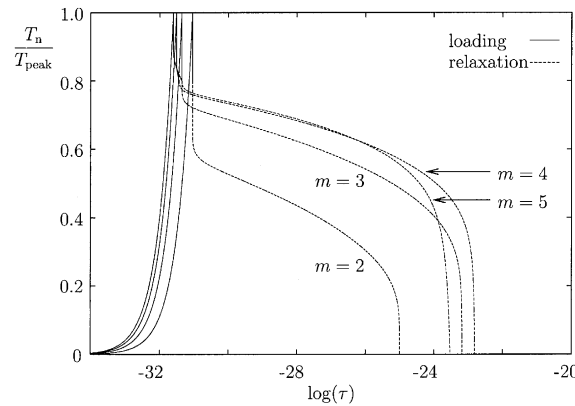
Fig. 3. Development of the traction T_n with dimensionless time τ for $n = 5$ and various values of m.
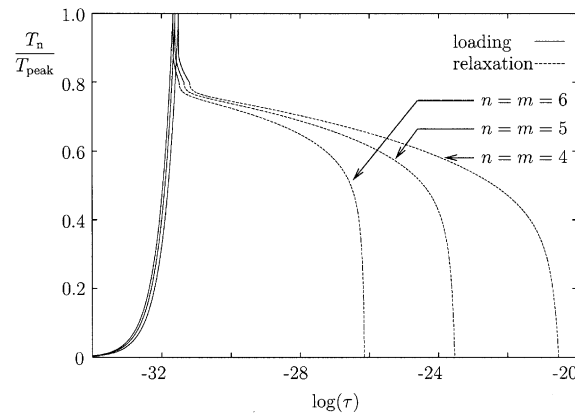

Fig. 4. Development of the traction T_n with dimensionless time τ for various values of $n = m$.

result of massive growth of microcracks simulated by the collective behavior of many cohesive surfaces. This effect cannot be taken into account in the model system. The values of n and m must therefore be calculated from the experiments in which creep plays a minor role. The experiments of Bažant and Gettu [5] with a high crack mouth opening rate therefore give the best comparison with the model system. From their Fig. 10 we obtain a relaxation initiation time of 5 s and a total relaxation time of 10^6 s, i.e. $t_2/t_1 = 10^{5.3}$.

From Fig. 4 we see that the model system gives a relaxation behavior with approximately $t_2/t_1 = 10^9$ for $n = m = 4$, $t_2/t_1 = 10^7$ for $n = m = 5$ and $t_2/t_1 = 10^5$ for $n = m = 6$. Taking into account considerable scatter in experimental results, one may conclude that if the model system must give a reasonable strain rate sensitivity, the values of n and m must be at least 5. Because of lack of more detailed knowledge, we here just take $n = m = 5$.

Now that the rate sensitivity of the model has been determined by n and m, peak load and fracture energy can be specified through the parameters T_0 and $\dot\omega_0$. A typical value for the Young's modulus of cement paste is $E = 20$ GPa. Using $k/E = 2500$ mm^{-1}, the cohesive surface stiffness is specified as $k = 50.0 \times 10^3$ GPa mm^{-1}. The relation between T_{peak}/T_0 and ku'/T_0 and between $G_f/T_0 u'$ and ku'/T_0 for $n = m = 5$ is shown
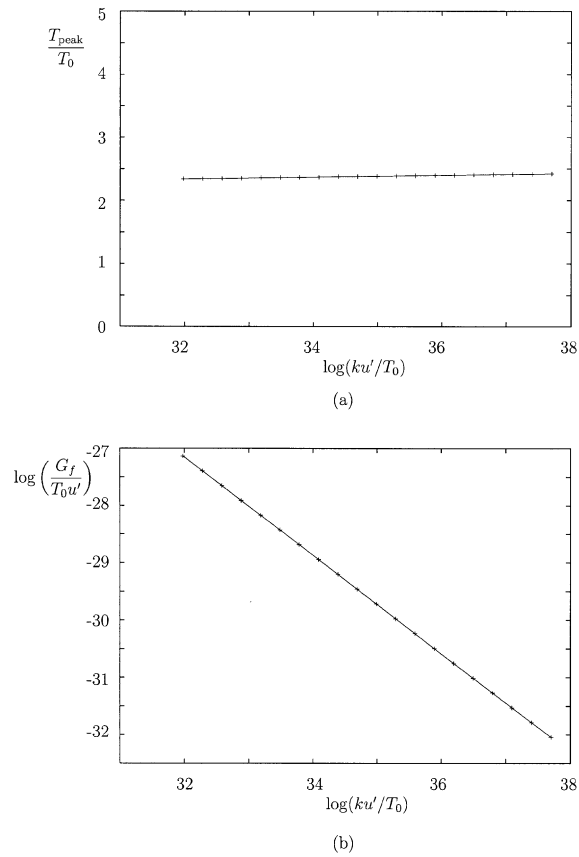
Fig. 5. The relation between (a) peak traction and driving force and (b) fracture energy and driving force as calculated from Eqs. (7) and (8).

in Fig. 5. For the values of m and n used here, the peak load is rather insensitive to variations in loading rate. Using these relations one finds for example that for a normalized loading rate $u' = 10^{28}$ and a reference traction $T_0 = 2.1$ MPa one obtains a peak traction $T_{peak} = 5$ MPa and a fracture energy $G_f = 19$ N mm^{-1}. Since $\dot{u} = \dot{\omega}_0 u'$, the values of T_{peak} and G_f are applicable to a strain rate of $\dot{\epsilon} = 10^{-7}$ if we choose $\dot{\omega}_0 = 10^{-35}$. Note that for higher strain rates the fracture energy increases. For example, the same parameters yield a fracture energy of 70 N mm^{-1} for $\dot{\epsilon} = 10^{-3}$.

For the fracture simulations for brittle heterogeneous materials to be presented hereafter, we have used the set of parameters given in Table 1. The parameter values in Table 1 result in the traction-separation relations given in Fig. 6 for a loading rate of $\dot{\epsilon} = 10^{-7}$ s^{-1}.

Note that the initial shape of the softening curve in Fig. 6 is similar to the softening curves that result from models describing the behavior of planar microcracks [17,18], i.e., a strong initial softening followed by a more gradual decrease of the cohesive surface traction. In our model, this is followed by breakdown of the cohesive surface in an accelerated manner which results in a cohesive surface opening at breakdown in the order of 0.01 mm. Although the precise values given in Table 1 are subject to debate, the ratio of the values of strength and fracture energy for the cement paste and ITZ are representative for cementitious composites.

Table 1
Bulk and cohesive surface parameters used in all calculations[a]

	Cement	Aggregate	Interface
E (GPa)	20	55	–
v	0.2	0.2	–
$\dot{\omega}_0$ (s^{-1})	10^{-35}	–	10^{-34}
T_0 (MPa)	2.1	–	0.9
m	5	–	5
n	5	–	5
σ_{max} (MPa)	5.0	–	2.1
G_f (N m^{-1})	19	–	3

[a] Peak load σ_{max} and fracture energy G_f are for a strain rate of $\dot{\epsilon} = 10^{-7}$ s^{-1}.
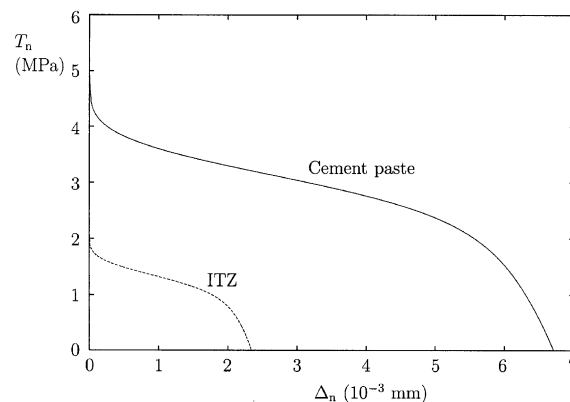
Fig. 6. Traction-separation relations for the cement paste and the ITZ for the material parameters given in Table 1 and a strain rate of 10^{-7} s^{-1}.

4. Computational modeling of fracture of a cementitious composite

On the level of observation that we are interested in here, with typical dimensions of a few millimeters, cementitious composites are highly heterogeneous materials consisting of a mix of cement paste and aggregates. In this paper we simplify this complex structure to a three phase material, i.e., aggregates embedded in a cementitious matrix and a weaker interfacial region separating aggregate and cement paste. It is important to realize that the ITZ in concrete has a finite thickness. In this work, the smallest aggregate is assumed to have a diameter of 0.25 mm. With a typical interfacial thickness of 30 μm we therefore take a minimum separation of 60 μm between aggregates. Since the interface thickness is an order of magnitude smaller than all other dimensions, the interfacial region can be collapsed into a cohesive surface and the region between aggregates consists of cement paste only. This assumption implies that interfacial cracks can only link up when a cement paste ligament between the aggregates fails. It should be noted that in concrete it may very well be possible that aggregates are so close to each other that interfacial regions are interconnected and form weak planes in the material. But here this possibility is excluded a priori.

The numerical generation of an aggregate structure for volume percentages typical for concrete (60% and higher) is difficult to achieve when randomly placing the aggregates in the material. A more realistic approach has been developed by Stroeven and Stroeven [19]. In short, the methodology randomly places aggregates in a computational window which is much larger than the desirable specimen size. Using random initial velocities for all aggregates, the computational window is shrunk accounting for the dynamic

contact interaction between aggregates until the specified volume percentage of aggregates is reached. The advantages of this methodology are evident in that very high volume percentages can be reached. Also, more realistic microstructures showing clustering of particles result from this approach. This clustering may have a significant influence on the fracture properties as compared to the properties of microstructures obtained by randomly placing aggregates.

Confining attention to brittle fracture in an elastic material, large strains are not to be expected in the bulk. However, finite strain effects may be of importance in the neighborhood of cracks. Using a Total Lagrangian description, incremental equilibrium is specified through the rate form of the principle of virtual work in the following form:

$$\Delta t \int_V (\dot{\tau}^{ij}\delta\eta_{ij} + \tau^{ik}\dot{u}^j_{,k}\delta u_{j,i})\,\mathrm{d}V + \Delta t \int_{S_i} \dot{T}_\alpha \delta \varDelta_\alpha \,\mathrm{d}S = \Delta t \int_{S_u} \dot{t}^i \delta u_i \,\mathrm{d}S - \left[\int_V \tau^{ij}\delta\eta_{ij}\,\mathrm{d}V + \int_{S_i} T_\alpha \delta \varDelta_\alpha \,\mathrm{d}S \right.$$
$$\left. - \int_{S_u} t^i \delta u_i \,\mathrm{d}S \right] \tag{10}$$

in which Δt is the time increment, V and S_u are the volume and outer surface of the body in the reference configuration and S_i is the current internal cohesive surface. The latter is the collection of all cohesive surface elements contained in V. The finite element equations are obtained by eliminating the stress rates $\dot{\tau}^{ij}$ using Eq. (1) and eliminating the cohesive surface traction rates using Eqs. (2) and (3).

In order to prevent the linear incremental time stepping scheme from drifting from the true equilibrium path, an equilibrium correction is taken into account. The term in Eq. (10) between square brackets represents the equilibrium correction which is zero for a state of perfect equilibrium.

In the discretization of the total cohesive surface area S_i, cohesive surface elements are used over the entire volume, as pioneered by Xu and Needleman [4]. In this way, crack initiation and propagation are independent of criteria other than the description of the failure processes in the cohesive surfaces. However, in this paper we are primarily interested in the simulation of multiple fracture in the cement matrix and the influence of the location and size of the aggregates. For this reason and for limiting CPU-time, the aggregates are assumed not to fracture. This limits the applicability of the results to normal strength concrete since penetration of cracks into aggregates, as often seen in high strength concretes, is precluded.

All calculations are two-dimensional under plane strain conditions. The aggregates are taken to be circular and we do not distinguish between volume and area percentages of aggregates. The specific fracture behavior of concrete seems to originate partly from the three-dimensional nature of concrete structures [20]. In three dimensions there is a larger freedom for crack bridges to form which inevitably leads to larger fracture energies and a higher ductility compared to the two-dimensional case. However, because of limited computational resources, such calculations must necessarily be postponed.

4.1. Development of fracture processes in a cementitious composite

The boundary value problem is illustrated in Fig. 7(a). A square block of cement paste having a width of 6 mm, containing 32 aggregates of diameter 0.25 mm, 16 aggregates of diameter 0.5 mm, 8 aggregates of diameter 1 mm and 4 aggregates of diameter 2 mm is loaded by a constant vertical displacement rate at the top face while restricting the bottom face in vertical direction. The specimen is free to contract horizontally. A typical finite element mesh is shown in Fig. 7(b). Continuum elements are given the properties of either the cement paste or aggregates according to the material parameters given in Table 1. Likewise, cohesive surfaces are given properties of cement paste unless they are located in between an aggregate and cement paste. In the latter case they are given properties of the interfacial transition zone (see Fig. 8).

Upon application of the vertical displacement at the top face of the specimen, damage develops in the cohesive surfaces as specified by the evolution Eq. (3). Due to the assumption that there is no initial damage
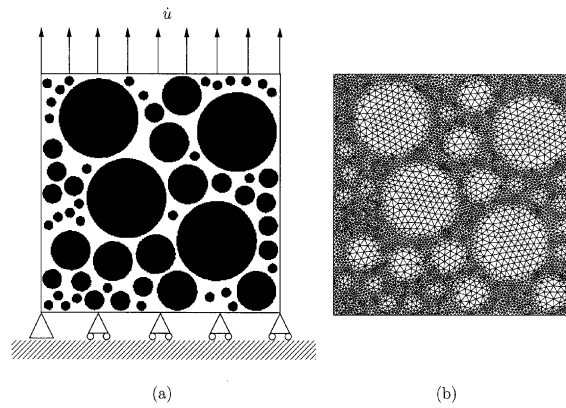
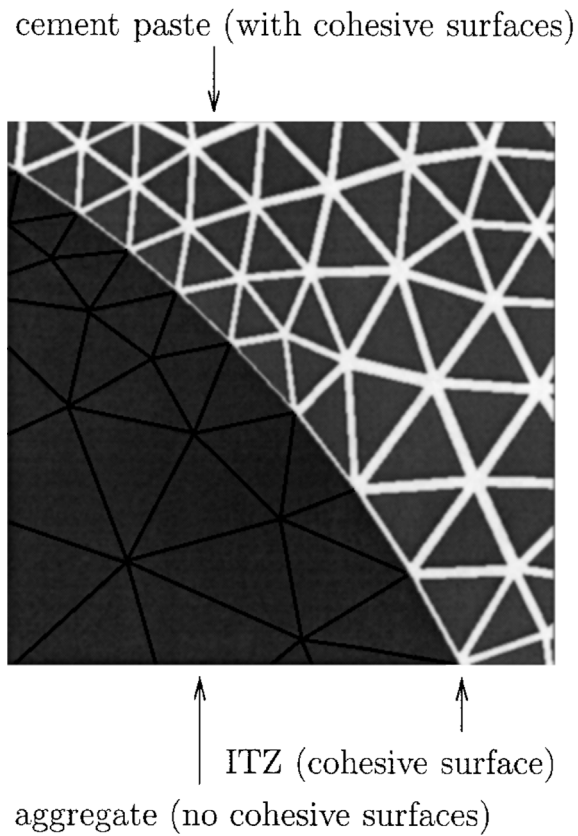Fig. 7. (a) Illustration of the boundary value problem of Section 4 and (b) finite element discretization.

Fig. 8. Representative part of a finite element mesh with embedded cohesive surfaces. The continuum elements have been shrunk for illustration purposes.

in the specimen, the rate at which damage evolves is very low at first, which results in a nearly linear elastic pre-peak response shown in Fig. 9. As the stresses become higher, more and more material in the specimen
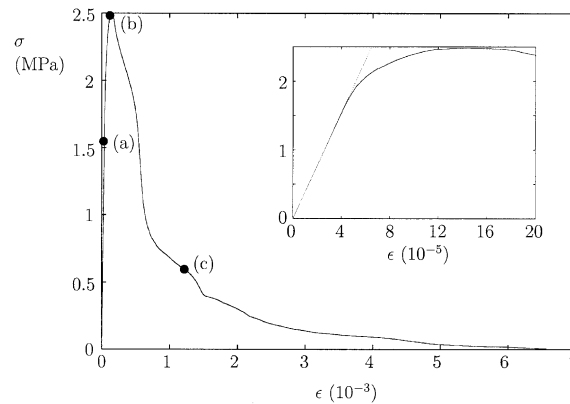
Fig. 9. Development of average stress at the top face of the specimen shown in Fig. 7. The onset of non-linearity, Fig. 10(a), local-ization of deformation, Fig. 10(b) and the start of resistance solely due to bridging, Fig. 10(c) are indicated.

becomes damaged. Since the ITZ is specified to be weaker then its surroundings and due to the stress concentrating effect of the stiffer aggregates, damage evolves faster on the poles of the aggregates. As shown in Fig. 10(a) and (b), before the peak stress is reached damage development is diffuse. This results in a noticeable deviation from linearity in the pre-peak regime, which for this specific microstructure starts at approximately 60% of the peak load.

Fig. 10(b) shows the distribution of damage at the onset of localization of deformation. At this point, the interfacial regions at the poles of all aggregates have failed almost completely. The hydrostatic stress distribution reveals that the aggregates have relaxed to a large extent and contribute less effectively to the load carrying capacity of the composite. The global fracture energy E_f (calculated as the total energy dissipation due to microcracking divided by the cross-section of the specimen) expanded in the fracture process up till peak load, i.e., the energy dissipated due to distributed microcracking, is 0.7 Nm m^{-2}. For the present case this amounts to roughly 5% of the total fracture energy (see Fig. 11). Once the peak is reached and the deformation starts to localize, the fracture energy increases to roughly 60% of its final value (from 0.7 to 8.0 Nm m^{-2}). At this point, nearly all cohesive surfaces spanning the crack have failed completely, i.e., the damage variable ω equals unity. We can thus conclude that all further resistance to loading has its origin in the bridges that form between the cracks (see Fig. 10(c)). From Fig. 11 it is clear that upon further loading, the fracture energy increases further up to a final value of 13.7 Nm m^{-2}.

The development of fracture in a cementitious composite is to a large extent dictated by the presence of the weak ITZ in between aggregates and cement matrix. Van Mier [20] has emphasized the occurrence of discontinuous crack growth, or bridging, in a cementitious composite. Since this implies a strong tendency for cracks to curve in order to link up, bridging strongly increases the fracture energy. The calculations show that discontinuous crack growth has its origin in the simultaneous degradation of material integrity at different locations. One or more of such damaged regions may eventually become dominant which results in multiple, disconnected cracks. The calculation for this specific microstructure furthermore shows that after localization of deformation, resistance due to bridging of the crack faces is responsible for a further increase in fracture energy of roughly 40%.

4.2. Effects of aggregate positioning

Crack deflection and meandering due to aggregates blocking the path of a crack may significantly in-crease the total fracture energy. To study the effect of aggregate positioning, 10 concrete mixes are created
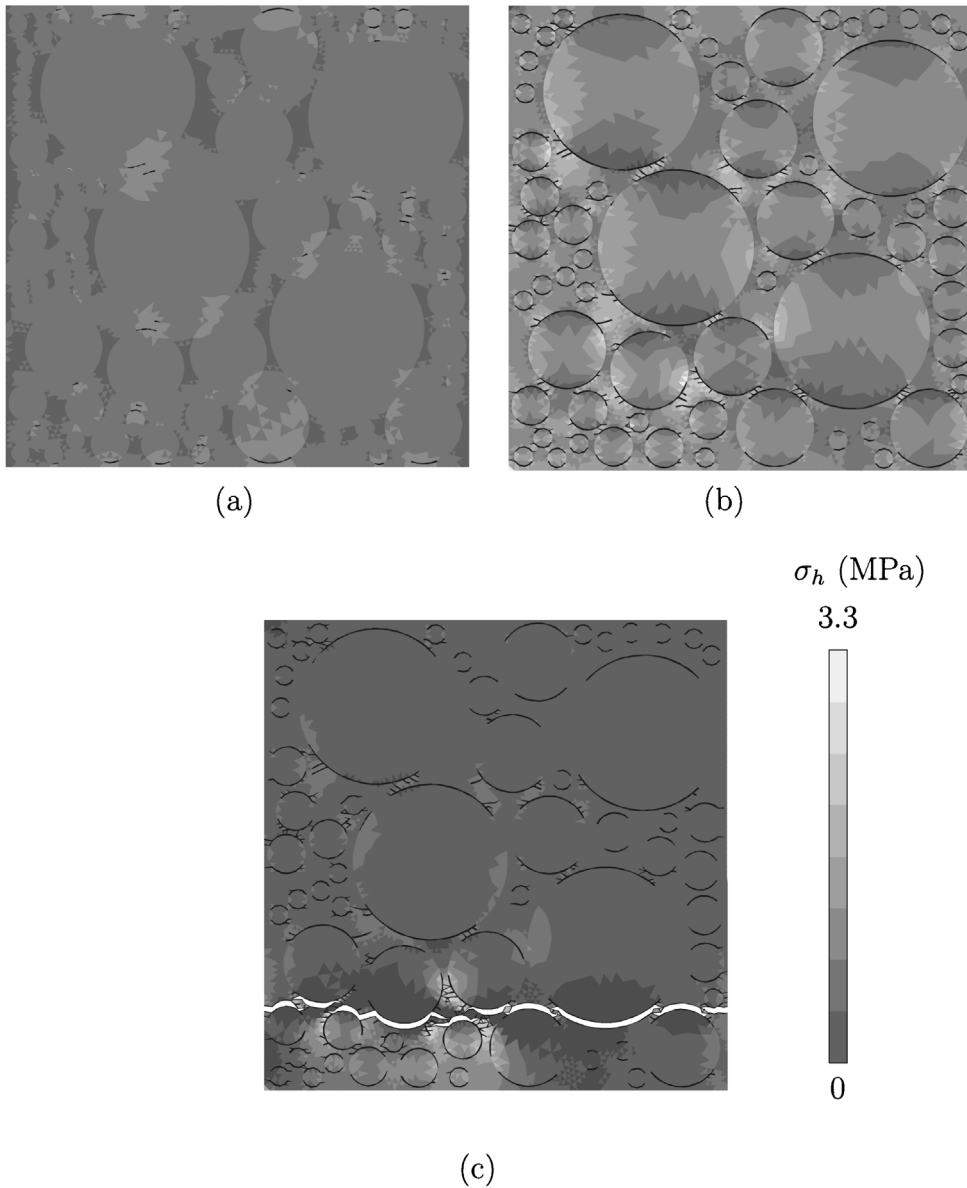
Fig. 10. Distribution of damage and hydrostatic stress σ_h (a) at the point of deviation from linearity in the pre-peak regime, (b) at the onset of localization and (c) at the point where all resistance against further loading comes from crack bridging. Displacements are magnified by a factor of 10.

all with the same aggregate diameters and number of aggregates as in Section 4.1. The volume fraction of aggregates is 66% for all mixes.

Two typical results are depicted in Fig. 12 at the point when the average vertical stress has decreased to 0.5 MPa. In Fig. 12(a) the specific distribution of aggregates results in a rather smooth fracture path because the dominant interfacial cracks are more or less aligned. This favors linking up of the cracks. However, in Fig. 12(b) one observes that the localization of deformation occurs in three larger cracks which
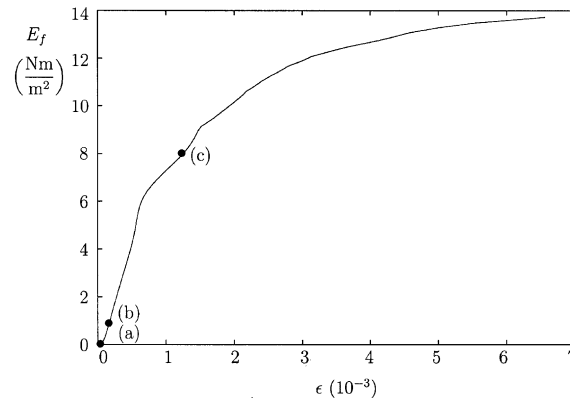
Fig. 11. Development of fracture energy per unit width of the specimen shown in Fig. 7. The onset of non-linearity, Fig. 10(a), localization of deformation, Fig. 10(b) and the start of resistance solely due to bridging, Fig. 10(c) are indicated.
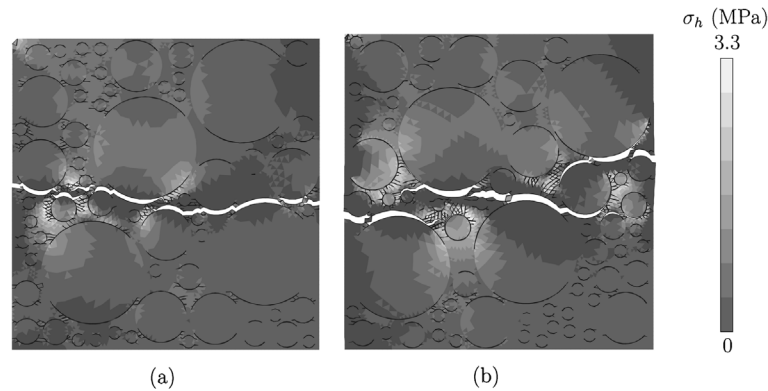

Fig. 12. Damage distribution and hydrostatic stress σ_h for two different arrangements of aggregates. Displacements are magnified by a factor of 10.

are not aligned and therefore linking up of the cracks is difficult. Large bridges of intact cement paste including smaller aggregates are formed which extend the lifetime of the specimen.

The relation between average vertical traction and strain for all 10 cases are given in Fig. 13. The peak tractions obtained with the various aggregate distributions range from 2.43 to 2.60 MPa, with a mean value of 2.54 MPa and a standard deviation of 0.06 MPa. Hence the differences between the various cases due to different aggregate arrangements are not significant during loading up to peak load. However, due to crack bridging, the fracture energies can differ significantly as shown in Fig. 14. Although final failure is hard to reach for certain arrangements due to numerical difficulties with the cohesive surface methodology, [1] it can be estimated from Fig. 14 that differences in fracture energy of up to 40% can occur.

---

[1] Since all continuum elements are separated from each other by cohesive surfaces, at some point during the simulation single elements or groups of elements may separate from the rest of the specimen. Under quasi-static conditions equilibrium can no longer be maintained and the calculation stops. This can be prevented by detecting such (groups of) elements before numerical problems arise, as done by Lingen and Tijssens [21] or by incorporating inertia effects.
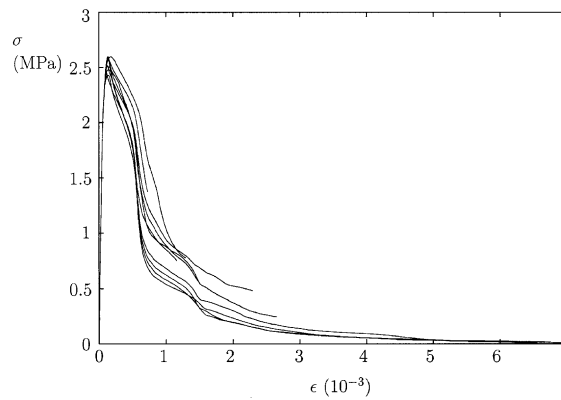
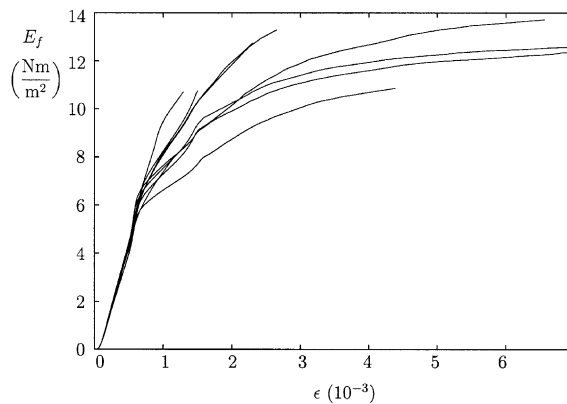Fig. 13. Average stress vs. strain for the mortar mixes of Section 4.2.

Fig. 14. Development of fracture energy as a function of strain for the various mortar mixes of Section 4.2.

4.3. Effect of loading rate

From experiments it is known that concrete shows a strong loading rate sensitivity. Experiments done by Bažant and Gettu [5] have clearly shown that for low loading rates the influence of creep on the deformation characteristics of concrete can be significant. Bažant et al. [6] have shown that the softening of concrete can be reversed to hardening if the loading rate is increased by a factor 1000.

To study the effects of the loading rate, a specimen with an aggregate volume fraction of 66% and a size distribution $d = 2:1:0.5:0.25$ mm of 1:8:28:32 is loaded by a strain rate of 10^{-4} s^{-1}. In the post-peak regime, the loading rate is changed by a factor ranging from 10^{-3} to 10^3. The stress–strain relations for these cases are shown in Fig. 15. For comparison purposes, the stress–strain curves for the same microstructure but for a constant strain rate of 10^{-7} and 10^{-1} s^{-1} are also shown.

The experiments by Bažant et al. [6] showed that upon a reduction of the loading rate by a factor 0.1 in the post-peak regime, the softening suddenly becomes much steeper for a short time. After this, the more gradual softening shown in the stress–strain relation before the decrease in loading rate is recovered. Bažant et al. [6] also showed that upon an increase in loading rate by a factor 1000 in the post-peak regime, a hardening response and a second peak are observed.
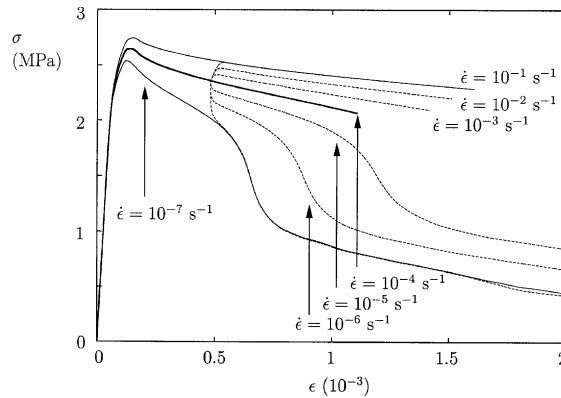
Fig. 15. Effect of change of strain rate on stress–strain relation. Strain rate is changed by factors of 10^{-3}–10^3 starting from $\dot{\epsilon} = 10^{-4}$ s^{-1}. For comparison, the stress–strain relations for $\dot{\epsilon} = 10^{-7}$ and 10^{-1} s^{-1} are also shown.

The numerical results shown in Fig. 15 are consistent with both experimental observations at least in a qualitative sense. The relaxation of the bulk due to growth of damage is determined by the stress state. Upon a decrease in loading rate the increase in elastic stresses suddenly becomes smaller whereas the initial relaxation progresses at the same rate. This causes the global stress level to decrease which in turn results in a lower relaxation rate because of a lower rate of increase of damage. As is evident from the curves for $\dot{\epsilon} = 10^{-7}$ s^{-1}, the global stress level relaxes to a level that coincides with the level that would have been obtained for a constant loading rate. The same applies for an increase in loading rate.

It must be noted that the change in loading rate in the present calculations was initiated in the post-peak regime, i.e. after localization of deformation. Since also no inertia effects are included, the fracture path does not change upon a change in loading rate. Including inertia effects may become important for example in the case where the loading rate was increased by a factor of 10^3 up to a strain rate of $\dot{\epsilon} = 10^{-1}$ s^{-1}. At such high strain rates, other complicating effects such as aggregate failure and the influence of moisture content and moisture diffusion may have an important influence on the outcome of the analysis.

4.4. Effect of relative contribution of aggregates

Taking the aggregate size distribution of Section 4.1 as a reference, we now substitute larger aggregates with smaller aggregates to investigate the effects of size distribution. Since the fracture processes of concrete are determined by the weaker interfacial zones, the microstructures are modified such that the interfacial area (approximately 100 mm^2) remains constant. Also, a constant aggregate volume fraction (66%) is used. This implies that the size of the specimen changes slightly. Within these constraints, one or more aggregates of diameter 2 mm are replaced by aggregates of diameter 0.25 or 0.5 mm. The evolution of the fracture energy as a function of global strain is given in Fig. 16(a), where the aggregates of diameter 2 mm are replaced by aggregates of diameter 0.25 mm and in Fig. 16(b) where this is done using aggregates of diameter 0.5 mm.

Comparing the curves in Fig. 16(a) with each other one observes that, upon replacing the larger aggregates by smaller aggregates, the fracture energy first increases and then decreases. In Fig. 16(b) one observes the opposite trend, i.e., the fracture energy first decreases and then increases. Hence from these results clear trends regarding the influence of smaller aggregates on the fracture energy as compared to larger aggregates cannot be deduced.
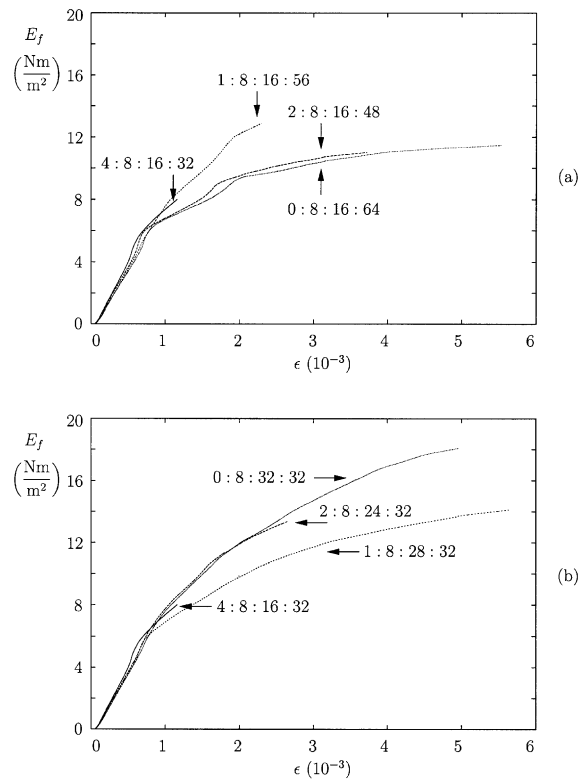
Fig. 16. Development of fracture energy as a function of strain for the mortar mix discussed in Section 4.4 in which aggregates of diameter 2 mm are replaced by aggregates of diameter (a) $d = 0.25$ and (b) $d = 0.5$ mm. The numbers equal the number of aggregates of size $d = 2:1:0.5:0.25$ mm.

The dominant role of crack bridging becomes apparent again in Fig. 17 in which the final crack patterns are given for four cases of Fig. 16. The large crack bridges shown in Fig. 17(c) and (d) contain a significant number of aggregates. Clearly the bridging mechanism dominates the global stress–strain behavior. Large scale computations are needed to investigate the influence of size distribution of aggregates on a larger scale of observation.

5. Concluding remarks

Cementitious composites fracture in a discontinuous way. Here, only microcracking due to external mechanical loading is considered, but in reality other effects such as drying–shrinkage cracking may occur as well. This will influence the location where fracture occurs and could possibly be taken into account through an initial damage distribution. Even apart from such complicating factors, cementitious composites are prone to develop multiple fractures at various sites in the material thus naturally generating crack bridges. These crack bridges are responsible for a significant increase in fracture energy. The calculations presented here reproduce numerically what was observed experimentally by Van Mier [20]. It should be noted, however, that the present results are applicable to a piece of material of only a few square millimeters. The maximum aggregate size assumed in the calculations is 2 mm and the calculations therefore represent fracture of mortar.
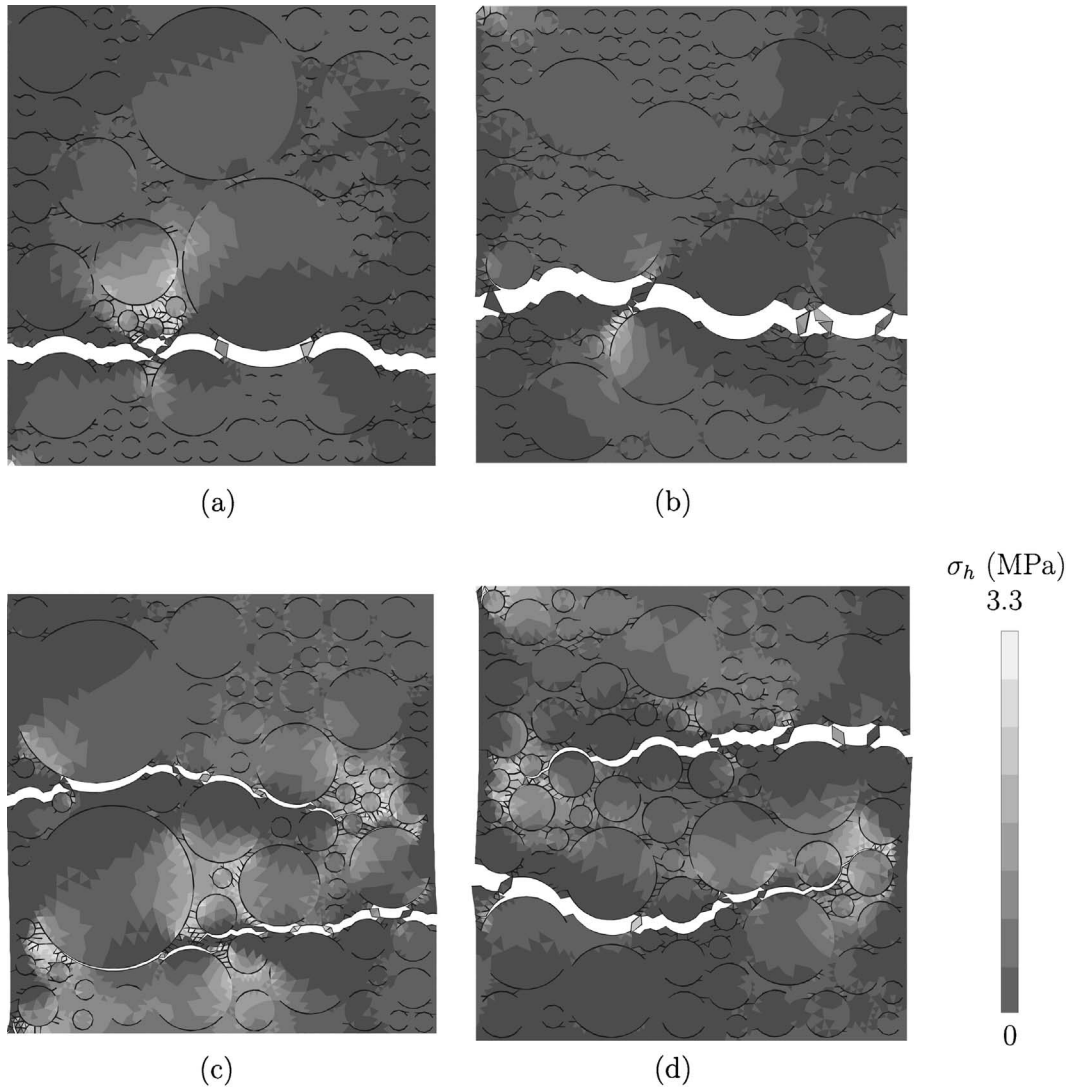
Fig. 17. Final fracture pattern and hydrostatic stress σ_h for the aggregate size distribution ($d = 2$:1:0.5:0.25 mm) (a) 2:8:16:48, (b) 0:8:16:64, (c) 2:8:24:32 and (d) 0:8:32:32. Also see Fig. 16. Displacements are magnified by a factor of 10.

The cohesive surface model presented in this paper is based on a traditional damage formulation and therefore does not directly link the micromechanical fracture events to the traction-separation relation of the cohesive surfaces. Nevertheless, the basic idea that planar microcracks evolve on a microscale and tend to grow in an accelerated manner seems to capture not only a reasonable softening relation for the cohesive surfaces but also results in realistic fracture path predictions on a mesoscale. Due to the extremely complex nature of the microstructure of cementitious composites, micromechanically based constitutive models for the mesolevel fracture behavior of concrete are not available yet and such models are necessary to make quantitatively correct predictions.

The results show that the fracture events in cementitious composites can be separated in three regimes, i.e., (i) the creation of many microcracks, mainly concentrated in the weaker interfacial transition regions,

(ii) the localization of deformation into multiple mesocracks and finally, (iii) the further growth of a true macrocrack, it being hindered by the bridging of intact pieces of mortar. The precise fracture characteristics are to a large extent dictated by the location of the aggregates.

Although experimental results suggest that concrete is a rate-dependent material and numerical simulations have been performed with viscoelastic constitutive models, the physical source of the rate dependence of the deformation of concrete is not clear. The rate dependence of the breaking of bonds is often said to be the source for the rate dependence of the constitutive response of concrete. However, experiments suggest that the moisture content also has a large influence on the observed rate dependence [9].

The effects of a change in loading rate qualitatively agree with what is observed in experiments. A steeper softening response is observed when the loading rate is decreased and a less steep softening or even re-hardening occurs when the loading rate is increased. However, in the present study, the aggregates are assumed not to fracture. Also, the fracture path did not change because the change in loading rate was initiated in the post-peak regime. A forthcoming paper will study the effect of loading rate in which aggregates can fracture. Since aggregates like limestone show hardly any strain rate dependence, the competition between fracture in the cement binder and the aggregates may have a significant influence on the final fracture path.

Comparable numerical simulations for fracture of concrete have been made with lattice models [22,23]. Such models qualitatively give the same results as obtained in our analysis, i.e. discontinuous crack growth due to crack growth initiation at multiple sites in the material. Although lattice models have clearly shown that discontinuous crack growth is a result of the disordered microstructure, the response obtained from crack growth simulations with lattice models is often too brittle. This can be attributed to the perfectly brittle fracture behavior which is often used in the lattice simulations. On the length scale on which lattice models are commonly used the assumption of brittle fracture may not be correct.

The cohesive surface methodology thus offers an alternative approach to study fracture events in heterogeneous materials. The effects of mesh alignment sensitivity, pointed out by Tijssens et al. [24] do not seem to dominate the solution in these kind of calculations due to the dominating effect of the stress field and the rather random creation of multiple discontinuous fractures.

Acknowledgements

References

[1] Hillerborg A, Modeer M, Petersson PE. Analysis of crack formation and crack growth in concrete by means of fracture mechanics and finite elements. Cement Concrete Res 1976;6:773–82.
[2] Bažant ZP, Li YN. Cohesive crack with rate-dependent opening and viscoelasticity. I. mathematical model and scaling. Int J Fract 1997;86:247–65.
[3] Tandon S, Faber KT, Bažant ZP, Yuan NL. Cohesive crack modeling of influence of sudden changes in loading rate on concrete fracture. Engng Fract Mech 1995;52:987–97.
[4] Xu X-P, Needleman A. Numerical simulations of fast crack growth in brittle solids. J Mech Phys Solids 1994;42:1397–434.
[5] Bažant ZP, Gettu R. Rate effects and load relaxation in static fracture of concrete. ACI Mater J 1992;89:456–68.
[6] Bažant ZP, Gu W-H, Faber KT. Softening reversal and other effects of a change in loading rate on fracture of concrete. ACI Mater J 1995;92:3–9.
[7] Yon J-H, Hawkins NM, Kobayashi AS. Strain-rate sensitivity of concrete mechanical properties. ACI Mater J 1992;89:146–53.
[8] Ross CA, Tedesco JW, Kuennen ST. Effects of strain rate on concrete strength. ACI Mater J 1995;92:37–47.

[9] Ross CA, Jerome DM, Tedesco JW, Hughes ML. Moisture and strain rate effects on concrete strength. ACI Mater J 1996;93: 293–300.

[10] Malvar LJ, Ross CA. Review of strain rate effects for concrete in tension. ACI Mater J 1998;95:735–9.

[11] Tobolsky A, Eyring H. Mechanical properties of polymeric materials. J Chem Phys 1943;11:125–34.

[12] Zurkov SN. Kinetic concept of the strength of solids. In: Yokobori T, Kawasaki T, Swedlow JL, editors. Proceedings of the First International Conference on Fracture, Sendai, Japan. vol. 2. 12–17 September, 1965. p. 1167–84.

[13] Kjellsen KO, Wallevik OH, Fjällberg L. Microstructure and microchemistry of the paste-aggregate interfacial transition zone of high-performance concrete. Adv Cement Res 1998;10:33–40.

[14] Kachanov M, Montagut ELE, Laures JP. Mechanics of crack-microcrack interactions. Mech Mater 1990;10:59–71.

[15] Koiter WT. An infinite row of collinear cracks in an infinite elastic sheet. Ingenieur Archiv 1959;28:168–72.

[16] Westmann RA. Asymmetric mixed boundary-value problems of the elastic half-space. J Appl Mech 1965;32:411–7.

[17] Ortiz M. Microcrack coalescence and macroscopic crack growth initiation in brittle solids. Int J Solids Struct 1988;24:231–50.

[18] Huang X, Karihaloo BL. Tension softening of quasi-brittle materials modelled by single and doubly periodic arrays of coplanar penny-shaped cracks. Mech Mater 1992;13:257–75.

[19] Stroeven M, Stroeven P. Computer-simulated internal structure of materials. Acta Stereologica 1996;15:247–52.

[20] Van Mier JGM. Mode I fracture of concrete: discontinuous crack growth and crack interface grain bridging. Cement Concrete Res 1991;21:1–15.

[21] Lingen FJ, Tijssens MGA. An efficient parallel procedure for the simulation of crack growth using the cohesive surface methodology. Int J Numer Meth Engng, submitted for publication.

[22] Schlangen E, Van Mier JGM. Experimental and numerical analysis of micro-mechanisms of fracture of cement-based composites. Cement Concrete Compos 1992a;14:105–18.

[23] Schlangen E, Van Mier JGM. Micromechanical analysis of fracture of concrete. Int J Damage Mech 1992b;1:435–54.

[24] Tijssens MGA, Sluys LJ, Van der Giessen E. Numerical simulation of quasi-brittle fracture using damaging cohesive surfaces. European J Mech A/Solids 2000;19:761–79.